https://doi.org/10.5194/acp-2020-93
Preprint. Discussion started: 19 February 2020

Atmospheric Chemistry and Physics Discussions

Impact of the South Asian monsoon outflow on atmospheric hydroperoxides in the upper troposphere

Bettina Hottmann[1], Sascha Hafermann[1], Laura Tomsche[1*†], Daniel Marno[1], Monica Martinez[1], Hartwig Harder[1], Andrea Pozzer[1], Marco Neumaier[2], Andreas Zahn[2], Birger Bohn[3], Helmut Ziereis[4], Jos Lelieveld[1] and Horst Fischer[1]

[1]Atmospheric Chemistry Department, Max Planck Institute for Chemistry, Mainz, 55128, Germany
[2]Karlsruhe Institute of Technology, Karlsruhe, 76021, Germany
[3]Forschungszentrum Jülich GmbH, Jülich, 52425, Germany
[4]German Aerospace Center, Institute of Atmospheric Physics, Oberpfaffenhofen, 82234, Germany
[*]now at NASA Langley Research Center, Hampton, VA 23681, USA
[†]now at Universities Space Research Association, Columbia, MD 21046, USA
Correspondence to: Bettina Hottmann (Bettina.Hottmann@mpic.de) and Horst Fischer (Horst.Fischer@mpic.de)

Abstract. During the OMO (Oxidation Mechanism Observation) mission, trace gas measurements were performed onboard the HALO (High Altitude LOng range) research aircraft in summer 2015 in order to investigate the outflow of the south Asian summer monsoon and its influence on the composition of the Asian Monsoon Anticyclone (AMA) in the upper troposphere over the eastern Mediterranean and the Arabian Peninsula. This study focuses on *in situ* observations of hydrogen peroxide (H_2O_2) and organic hydroperoxides (ROOH), as well as their precursors and loss processes. Observations are compared to steady state calculations of H_2O_2, methyl hydroperoxide (MHP) and inferred unidentified hydroperoxide (UHP) mixing ratios. Measurements are also contrasted to simulations with the general circulation ECHAM/MESSy for Atmospheric Chemistry (EMAC) model. We observed enhanced mixing ratios of H_2O_2, MHP and UHP in the AMA relative to the northern hemispheric background. Highest concentrations for H_2O_2 and MHP were found in the southern hemisphere outside the AMA, while for UHP, highest concentrations were found within the AMA. In general, the observed concentrations are higher than steady-state calculations and EMAC simulations. Especially in the AMA, EMAC underestimates the H_2O_2 and ROOH mixing ratios. Longitudinal gradients indicate a pool of hydroperoxides towards the center of the AMA, most likely associated with upwind convection over India. This indicates main contributions of atmospheric transport to the local budgets of hydroperoxides along the flight track, explaining strong deviations to steady-state calculations which only account for local photochemistry. Deviations to EMAC simulations are most likely due to uncertainties in the scavenging efficiencies for individual hydroperoxides in deep convective transport to the upper troposphere, corroborated by a sensitivity study. It seems that the observed excess UHP is excess MHP transported to the west from an upper tropospheric source related to convection in the summer monsoon over South-East Asia.

https://doi.org/10.5194/acp-2020-93
Preprint. Discussion started: 19 February 2020

Atmospheric Chemistry and Physics Discussions

1 Introduction

The earth has an oxidizing atmosphere where OH functions as the main oxidizing agent (Levy, 1971). OH is formed by the photolysis of ozone (λ<320 nm) and subsequent reaction of the produced singlet D oxygen atom (O^1D) with water vapor. The main sinks of OH are also the main sources of peroxy radicals (HO_2 and RO_2) in the reactions with CO, CH_4 and volatile organic compounds (VOCs) and the reaction with nitrogen dioxide (NO_2) to form nitric acid (HNO_3). At low NO_x ($NO+NO_2$) concentrations, HO_2 reacts with itself to form H_2O_2 or with RO_2 to form organic hydroperoxides (ROOH). Since HO_2 and RO_2, especially CH_3O_2, react faster with NO than with HO_2, peroxides are mainly produced in areas with low NO and high OH mixing ratios (Lee et al., 2000). H_2O_2 is a strong oxidant in the aqueous phase, oxidizing for example SO_2 to H_2SO_4, and hence H_2O_2 partially contributes to acid rain formation (e.g. Hoffmann and Edwards, 1975; Penkett et al., 1979; Robbin Martin and Damschen, 1981; Calvert et al., 1985). The major photochemical sinks of hydroperoxides are photolysis, which recycles OH, and the reaction with OH forms HO_2. Physical loss of hydroperoxides due to dry and wet deposition establishes an ultimate loss mechanism of HO_x radicals. Thus H_2O_2 and ROOH play a pivotal role to the HO_x-budget and modulate the oxidation capacity of the atmosphere (Lelieveld and Crutzen, 1990; Crutzen et al., 1999).

The global distribution of hydroperoxides is affected by transport, physical removal by dry deposition and rainout as well as net photochemical production processes. With increasing altitude, and thus decreasing water vapor concentration, the primary production of HO_x decreases (Heikes et al., 1996) and leads to an increasing contribution of the photolysis of H_2O_2 and ROOH to the HO_x budget (Jaeglé et al., 1997; Jaeglé et al., 2000; Faloona et al., 2000; Faloona et al., 2004). In more polluted areas, especially in the boundary layer, the H_2O_2 chemistry is more complex and leads to higher variabilities (Nunnermacker et al., 2008). Close to the surface dry deposition of H_2O_2 forms a strong sink resulting in decreasing concentrations with decreasing altitude. This often leads to a local maximum of H_2O_2 mixing ratios above the boundary layer at 2–5 km of altitude (Daum et al., 1990; Heikes, 1992; Weinstein-Lloyd et al., 1998; Snow, 2003; Snow et al., 2007; Klippel et al., 2011). A similar but weaker maximum at 2–5 km was found for methyl hydroperoxide (MHP) (Weinstein-Lloyd et al., 1998; Snow, 2003; Snow et al., 2007). Due to its lower deposition velocity associated with less efficient uptake by solid and aqueous surfaces, MHP is not as sensitive to deposition processes as H_2O_2 (Lind and Kok, 1986, 1994), yielding rather constant mixing ratios with altitude within the boundary layer. Further, the mixing ratios of both species generally decrease with increasing latitude in the free troposphere due to lower water vapor concentrations (Jacob and Klockow, 1992; Perros, 1993; Slemr and Tremmel, 1994; Snow, 2003; Snow et al., 2007; Klippel et al., 2011).

In spite of several *in situ* measurement campaigns of trace gases in the outflow of the Asian summer monsoon in the recent years, e.g. from the IAGOS-CARIBIC project (Ojha et al., 2016; Rauthe-Schöch et al., 2016), the IAGOS-MOZAIC project (Barret et al., 2016), the MINOS aircraft campaign (Lelieveld et al., 2002) and the PEM-WEST A mission (Heikes et al., 1996) our understanding of the physical and chemical processes within the Asian Monsoon Anticyclone (AMA) is limited. Since the Asian summer monsoon has a strong influence on the upper troposphere (UT) and the lower stratosphere (Randel et al., 2010; Gettelman et al., 2004), it is important to study its physical and chemical properties in greater detail.

https://doi.org/10.5194/acp-2020-93
Preprint. Discussion started: 19 February 2020


Atmospheric Chemistry and Physics Discussions

The focus of the OMO (Oxidation Mechanism Observation) campaign was to investigate photochemical processes in the AMA in the UT. During the mission, HALO probed a large variety of air masses, ranging from clean northern hemispheric (NH) background air above the western Mediterranean, southern hemispheric (SH) background air over the northern Indian Ocean and air masses affected by the South Asian summer monsoon in the AMA over the Arabian Peninsula. The main goals of the campaign were to analyze the influence of the AMA on the oxidizing power of the atmosphere and to determine the rates at which natural and human-made compounds are converted by oxidation processes in the atmosphere (Lelieveld et al., 2018).

The present study addresses the budgets of H_2O_2 and organic hydroperoxides. Since the measurements of organic hydroperoxides are unspecific, we estimate the contribution from methyl hydroperoxide (MHP) based on steady-state calculations. In former studies MHP was identified as the most abundant organic hydroperoxide in the free troposphere (Heikes et al., 1996; Jackson and Hewitt, 1996). Our goal was to investigate to what extent this is also the case for the outflow of the South Asian summer monsoon into the UT. In addition the *in situ* data were compared to results from the EMAC model (see 3.5) along the flight track for H_2O_2 and individual ROOH mixing ratios. Observed H_2O_2 mixing ratios were also evaluated with steady-state calculations based on measured HO_x and photolysis frequency measurements onboard of HALO.

2 The OMO project

The OMO campaign took place from 21st of July to 27th of August 2015. During the campaign 17 flights with the HALO (High Altitude and LOng range) research aircraft were performed. The airports of Oberpfaffenhofen (Germany), Paphos (Cyprus), Gan (Maldives) and Bahrain served as bases for take-offs and landings. The flights were mainly performed over the Arabian Peninsula, the Eastern Mediterranean and the Northern Indian Ocean (11.3–80.2°E and 0.2°S–48.1°N). In Figure 1 the tracks of all OMO flights are shown. The aircraft reached altitudes up to 15 km which corresponds to 130 hPa to study the chemistry of the UT.

3 Methods

3.1 Hydroperoxide measurements

The hydroperoxide data during OMO were obtained using a modified commercial instrument (AEROLASER, model AL2021, Garmisch-Partenkirchen, Germany) called HYPHOP (HYdrogen Peroxide and Higher Organic Peroxides monitor). The HYPHOP-instrument was installed in a 19″ rack together with the IR-laser absorption instrument TRISTAR (Tracer *In Situ* Tdlas for Atmospheric Research) mounted in the back of HALO. Air was sampled from the top of the aircraft fuselage through a forward-facing trace gas inlet (TGI) designed as a bypass, consisting of a ½" PFA (perfluoroalkoxy alkanes) tube inside the aircraft with an exit through a second TGI. From this bypass air was sampled at a flow rate of 2 slpm (standard

https://doi.org/10.5194/acp-2020-93
Preprint. Discussion started: 19 February 2020


Atmospheric Chemistry and Physics Discussions

liter per minute) through a ¼" PFA tube and directed to HYPHOP. To obtain constant pressure at the HYPHOP inlet a constant pressure inlet (CPI) consisting of a dual stage membrane pump (Vacuubrand MD1C VARIO SP, Wertheim, Germany) was used (Klippel et al., 2011).

HYPHOP relies on a dual enzyme detection method after transfer of gaseous hydroperoxides into a buffered solution (potassium hydrogen phthalate/NaOH, pH 6) in a glass stripping coil (Lazrus et al., 1985; Lazrus et al., 1986). This stripper also contains EDTA (ethylenediaminetetraacetic acid) to prevent the reaction of transition metal ions with the hydroperoxides. Additionally, formaldehyde (HCHO) is added to prevent the oxidation of dissolved SO_2 (in alkaline solutions HSO_3^-) by the hydroperoxides. Instead, HCHO and HSO_3^- form hydroxymethyl sulfonate ($HOCH_2SO_3^-$). After the stripping coil the hydroperoxide containing solution is divided into two channels. Catalase is added to one channel in order to selectively destroy H_2O_2. This first channel thus measures only ROOH, while the second channel (without catalase) measures the sum of ROOH and H_2O_2. Since hydroperoxides cannot be detected by fluorescence directly, a second enzyme (horseradish peroxidase) and *p*-hydroxyphenylacetic acid (POPHA) are added to both channels. In a quantitative and selective reaction the enzyme catalyzes the oxidation of POPHA by hydroperoxides forming the fluorescent dye 6,6'-dihydroxy-3,3'-biphenyldiacetid acid. After excitation at 326 nm with a Cd lamp, the fluorescence at 400–420 nm is detected. To enlarge the fluorescence intensity sodium hydroxide is added.

In order to perform zero measurements, the sampled air is directed through a cylinder filled with hopcalite (MnO_2 and CuO) to eliminate H_2O_2, ROOH and Ozone. Since the efficiency of Hopkalit decreases with increased humidity, the air is dried beforehand with the help of orange gel (SiO_2 beads plus indicator).

To convert the detected signal into a concentration a 4-point calibration was performed before and after every flight. In the first two steps a liquid standard of H_2O_2 (1 µmol/L, freshly diluted from stock solution) followed by zero air is measured in both channels without catalase. Afterwards this is repeated with catalase in the ROOH channel for the last two steps. The sensitivity for both channels and the catalase efficiency are determined via this procedure. The concentration of the liquid standard is based on titration of the stock solution (10 mmol/L) with potassium permanganate.

To determine the stripping efficiency for H_2O_2, a gas phase standard based from a permeation source (Teflon tube filled with 30% H_2O_2 in a temperature-controlled glass flask) is used at a constant flow rate of approximately 40 sccm diluted with synthetic air and measured with the instrument. The permeation rate of the source is quantified by collecting the output of the source into cooled water. The addition of hydrochloric titanium tetrachloride yields the formation of the yellow η^2-peroxo complex $[Ti(\eta^2\text{-}O_2)Cl_4]^{2-}$ (Pilz and Johann, 1974) whose concentration is determined via a UV photometer. The stripping efficiency of MHP was assumed to be 60% and that of H_2O_2 100% (AEROLASER, 2006; Lee et al., 2000).

The inlet efficiency was determined with the help of the permeation source which was measured with and without the CPI. In laboratory studies the inlet efficiency was determined to be 87% ± 3% decreasing during the campaign to 62.7% ± 0.8%, which is mainly due to the higher humidity.

https://doi.org/10.5194/acp-2020-93
Preprint. Discussion started: 19 February 2020


Atmospheric Chemistry and Physics Discussions

The limits of detection (LOD) and precisions for H_2O_2 and MHP (assuming total ROOH to be mainly MHP), respectively, have been calculated for each flight from the reproducibility (1σ standard deviation) of in-flight zero (650 values) and liquid calibration (100 values) measurements, taking into account the sensitivity, stripping and catalase efficiency. Values for the LOD are in the range of 8–53 ppt_v for H_2O_2 (median 23 ppt_v) and 9–52 ppt_v for MHP (median 23 ppt_v) respectively. Precision values were determined from the reproducibility of standard measurements and are in the range of 0.2%@5.2 ppb_v and 1.3%@5.9 ppb_v for H_2O_2 and 0.3%@5.0 ppb_v and 2.1%@6.0 ppb_v for MHP. The time resolution (signal increase from 10% to 90%) of the instrument is 120 s. An ozone interference of 53 ppt_v H_2O_2 per 100 ppb_v O_3, which was determined by H_2O_2 measurements in the stratosphere during the OMO-EU test campaign, was taken into account and corrected.

The total uncertainty calculated from statistical errors and uncertainties of liquid standard, inlet and stripping efficiency and ozone interference is 25% for H_2O_2 and 40% for MHP.

3.2 Other *in situ* measurements

For this study CO, CH_4, HO_x, O_3, Acetone, NO_y, J_{H2O2} and J_{MHP} data measured by other instruments have been used for data interpretation, steady-state calculations and interference corrections (see section 3.1). CO and CH_4 have been measured by the IR-quantum cascade laser absorption spectrometer TRISTAR (Schiller et al., 2008; Tadic et al., 2017). The measurements comprised an ambient air mode and in-flight calibrations. The latter were realized with secondary standards from pressurized bottles (6 L bottle, Auer GmbH, Germany), which were calibrated against certified reference gases (Tomsche et al., 2019). With the help of the in-flight calibrations the *in situ* data are drift-corrected by interpolation between two calibrations (Tadic et al., 2017). The observed CO and CH_4 mixing ratios have a total uncertainty of 5.1% and 0.275%, respectively. The relatively high CO uncertainty reflects problems with the stability of the CO quantum cascade laser during the second half of OMO.

Laser induced fluorescence was the method utilized for HO_x measurements (instrument name: HORUS, Faloona et al., 2004; Martinez et al., 2010). The accuracies of the measurements are 17.1% for OH and 17.6% for HO_2. The limit of detection of the instrument does vary depending on altitude as this system has a sensitivity that depends on pressure. As altitude increases the LOD decreases from 0.1 ppt_v to 0.02 ppt_v for OH and 0.361 ppt_v to 0.175 ppt_v for HO_2.

FAIRO (Fast AIRborne Ozone instrument) is a light-weight (14.5 kg) and accurate 2-sensor device for measuring O_3. It combines two techniques, i.e. (a) a UV photometer that measures the light absorption by O_3 at a wavelength of λ = 250–260 nm emitted by a UV-LED and (b) a chemiluminescence detector that monitors the chemiluminescence generated by O_3 on the surface of an organic dye adsorbed on dry silica gel. These techniques are simultaneously applied in order to combine the high measurement accuracy of the UV photometry with the high measurement frequency of the chemiluminescence detection. The UV photometer has a 1-σ precision of 0.08 ppb_v at a measurement frequency of 0.25 Hz (and a pressure of 1 bar) and an accuracy of 1.5% (determined by the uncertainty of the O_3 cross section). The chemiluminescence detector has a precision of 0.05 ppb_v at a measurement frequency of 12.5 Hz (Zahn et al., 2012). In post-processing the chemiluminescence detector data is calibrated using the UV photometer data.

https://doi.org/10.5194/acp-2020-93
Preprint. Discussion started: 19 February 2020


Atmospheric Chemistry and Physics Discussions

Nitrogen oxide (NO) and total reactive nitrogen (NO_y) were measured using the AENEAS-atmospheric nitrogen oxides measuring system. The measurements were performed by a dual channel NO-chemiluminescence detector (CLD-SR 790, Eco Physics, Switzerland) in combination with a converter technique for the detection of total reactive nitrogen as NO. NO_y comprises among others NO, NO_2, HNO_3, NO_3, N_2O_5, HNO_2, HO_2NO_2, PAN and organic nitrates. The individual NO_y species were detected after conversion to NO using a gold tube maintained at about 300 °C with H_2 as a reducing agent (Ziereis et al., 2000). Ambient air was sampled using a standard HALO trace gas inlet equipped with a heated (~ 40 °C) PFA inlet line. The time resolution of the measurements was about 1 s. The overall uncertainty of the NO and NO_y measurements depends on its ambient concentrations and is about 8% (6.5%) for volume mixing ratios of 0.5 nmol/mol (1 nmol/mol), respectively (Stratmann et al., 2016).

VOCs (e.g. acetone) were measured with a homebuilt light-weight (~55 kg without rack) proton-transfer-reaction mass spectrometer which uses a commercial quadrupole mass analyzer (Pfeiffer, QMA 410, Germany). A modular V25 micro computer system (MPI-C, Mainz, Germany) is applied for instrument control and data acquisition. A custom-built inlet system comprises a platinum/quartz wool scrubber (Shimadzu, High Sensitivity Catalyst) held at 300 °C and components for flow and pressure control. The instrument was calibrated between flights with a dynamically diluted gas standard containing approximately 500 ppb_v of VOCs (Apel-Riemer Environmental Inc., USA). The accuracy for acetone is typically ±10% and the detection limit is ~60 ppt_v.

Photolysis frequencies were calculated from spectral actinic flux density spectra (280–650 nm) obtained from CCD spectroradiometer measurements on the top and bottom fuselage of the aircraft covering the upper and the lower hemisphere, respectively (Bohn and Lohse, 2017). Recent recommendations of absorption cross sections and quantum yields were used in the calculations, as well as their temperature and pressure dependencies (if available) by taking into account measured static air temperatures and pressures. Radiometric uncertainties range around 5–6% under typical flight conditions. Additional uncertainties related to the molecular parameters are process specific. For H_2O_2 in particular, recommended absorption cross sections and their temperature dependencies were applied and unity quantum yields were assumed (Burkholder et al., 2015). However, the recommended H_2O_2 absorption cross sections are confined to a wavelength range below 350 nm which is insufficient to capture atmospheric photolysis completely. Because measured cross sections decay exponentially over two orders of magnitude in the range 280–350 nm, this dependence was further extrapolated up to 370 nm where values drop well below 10^{-22} cm^2. Dependent on conditions this extrapolation increases atmospheric H_2O_2 photolysis frequencies by 10–20%. For MHP the temperature dependence of the absorption cross sections is unknown. Therefore the recommended room temperature data were used under all conditions as well as unity quantum yields (Burkholder et al., 2015). Combined total uncertainties of 15% and 25% are estimated for H_2O_2 and MHP photolysis frequencies, respectively.

Latitude, longitude and altitude data were collected with the BAHAMAS (BAsic HALO Measurement And Sensor system) instrument. More detailed information about the installation of scientific instruments and mission flights can be found on http://www.halo.dlr.de/science/missions/omo/omo.html.

https://doi.org/10.5194/acp-2020-93
Preprint. Discussion started: 19 February 2020

Atmospheric Chemistry and Physics Discussions

3.3 Photo-stationary state calculations

Since only the sum of organic hydroperoxides was measured we estimated the contribution of MHP using a photo-stationary-state (PSS) approximation relying on *in situ* measurements of HO_2, OH, CO, CH_4, NO, J_{MHP} and J_{H2O2} (see 3.2) and rate coefficient data from Atkinson et al. (2004 and 2006).

In the free troposphere the production rate P of H_2O_2 and MHP is due to the self-reaction of HO_2 and reaction of CH_3O_2 with HO_2, respectively, and can be calculated from Eq. 1 and 2.

$$P(H_2O_2) = k_{HO_2+HO_2} \cdot [HO_2]^2 \,, \quad (1)$$

$$P(MHP) = k_{CH_3O_2+HO_2} \cdot [CH_3O_2] \cdot [HO_2] \,, \quad (2)$$

Photochemical loss rates L of H_2O_2 and MHP are due to photolysis and reaction with OH according to Eq. 3 and 4.

$$L(H_2O_2) = \left(k_{H_2O_2+OH} \cdot [OH] + J_{H_2O_2}\right) \cdot [H_2O_2] \,, \quad (3)$$

$$L(MHP) = (k_{MHP+OH} \cdot [OH] + J_{MHP}) \cdot [MHP] \,, \quad (4)$$

For steady-state conditions the production and loss reactions are at equilibrium and the MHP to H_2O_2 ratio can be calculated from Eq. 5.

$$\frac{[MHP]}{[H_2O_2]} = \frac{k_{CH_3O_2+HO_2} \cdot [CH_3O_2] \cdot [HO_2]}{k_{HO_2+HO_2} \cdot [HO_2]^2} \cdot \frac{k_{H_2O_2+OH} \cdot [OH] + J_{H_2O_2}}{k_{MHP+OH} \cdot [OH] + J_{MHP}} \,, \quad (5)$$

Similarly the CH_3O_2 to HO_2 ratio can be deduced from Eq. 6.

$$\frac{[CH_3O_2]}{[HO_2]} = \frac{L(HO_2) \cdot P(CH_3O_2)}{P(HO_2) \cdot L(CH_3O_2)} \,, \quad (6)$$

Dominant loss processes for HO_2 and CH_3O_2 are reactions with NO and the production of H_2O_2 and MHP, respectively, neglecting the production of peroxy nitrates due to low NO_2 concentrations in the UT (Eq. 7 and 8).

$$L(HO_2) = k_{CH_3O_2+HO_2} \cdot [CH_3O_2] \cdot [HO_2] + k_{HO_2+NO} \cdot [HO_2] \cdot [NO] + k_{HO_2+HO_2} \cdot [HO_2]^2 \,, \quad (7)$$

$$L(CH_3O_2) = k_{CH_3O_2+HO_2} \cdot [CH_3O_2] \cdot [HO_2] + k_{CH_3O_2+NO} \cdot [CH_3O_2] \cdot [NO] \,, \quad (8)$$

The first terms on the right side of both equations are identical. The second terms are dominated by the rate coefficients of the reactions with NO and the NO concentration. For the calculations of the rate coefficients the mean temperature of 259.18 K, the mean altitude of 10,992.8 m and a scale height of 7,400 m were used. The resulting values are shown in Eq. 9–11.

$$k_{HO_2+NO} = 3.45 \cdot 10^{-12} \cdot \exp^{\frac{270}{T}} = 9.78 \cdot 10^{-12} \frac{cm^3}{molecule \cdot s} \,, \quad (9)$$

$$k_{CH_3O_2+NO} = 2.3 \cdot 10^{-12} \cdot \exp^{\frac{360}{T}} = 9.22 \cdot 10^{-12} \frac{cm^3}{molecule \cdot s} \,, \quad (10)$$

$$k_{HO_2+HO_2} = 2.2 \cdot 10^{-13} \cdot \exp^{\frac{600}{T}} + 1.9 \cdot 10^{-33} \cdot [N_2] \cdot \exp^{\frac{980}{T}} = 2.64 \cdot 10^{-12} \frac{cm^3}{molecule \cdot s} \,, \quad (11)$$

This indicates that the reaction of HO_2 with NO is more than a factor of 3 faster than the self-reaction. The measured NO concentration is an order of magnitude larger than measured HO_2, so that reaction with NO is the dominant process for both

https://doi.org/10.5194/acp-2020-93
Preprint. Discussion started: 19 February 2020


Atmospheric Chemistry and Physics Discussions

HO_2 and CH_3O_2 resulting in similar loss rates for both radicals in the UT. Thus, the ratio of CH_3O_2 to HO_2 is dominated by their production rates (Eq. 12).

$$\frac{[CH_3O_2]}{[HO_2]} = \frac{P(CH_3O_2)}{P(HO_2)} = \frac{k_{CH_4+OH}\cdot[CH_4]\cdot[OH]}{k_{CO+OH}\cdot[CO]\cdot[OH]}, \quad (12)$$

The combination of Eq. 5 and 12 yields in Eq. 13 which was used to calculate the MHP concentrations.

$$[MHP] = \frac{k_{CH_3O_2+HO_2}}{k_{HO_2+HO_2}} \cdot \frac{k_{H_2O_2+OH}\cdot[OH]+J_{H_2O_2}}{k_{MHP+OH}\cdot[OH]+J_{MHP}} \cdot \frac{k_{CH_4+OH}\cdot[CH_4]}{k_{CO+OH}\cdot[CO]} \cdot [H_2O_2], \quad (13)$$

Please note that other sources of HO_2 and CH_3O_2, in particular the photolysis of formaldehyde (HCHO) and acetaldehyde, respectively have been neglected. This is justified by the generally low mixing ratios of these species at high altitudes.

The total uncertainty of MHP from the calculation according to equation 13 can be deduced from error propagation taking into account uncertainties in rate constants, OH (17.1%), J_{H2O2} (15%), J_{MHP} (25%), CH_4 (0.275%), CO (5.1%) and H_2O_2 (25%) to be of the order of 45% (1σ).

To estimate the composition of the organic hydroperoxides the calculated concentration of MHP was subtracted from the measured sum of all organic hydroperoxides. This leads to a concentration of unidentified organic hydroperoxides (UHP) (Eq. 14).

$$[UHP] = [ROOH] - [MHP], \quad (14)$$

3.4 H_2O_2 calculation

In order to classify the measured H_2O_2, HO_2 and OH data we calculated H_2O_2 from measured HO_x and J_{H2O2}. For the calculation Eq. 15 was used which is based on Eq. 1 and Eq. 3.

$$[H_2O_2]_{PSS} = \frac{[HO_2]^2\cdot k_{HO_2}}{[OH]\cdot k_{OH}+J_{H_2O_2}}, \quad (15)$$

A total uncertainty of 45% (1σ) due to uncertainties in reaction rate constants, OH (17.1%), HO_2 (17.6%) and J_{H2O2} (15%) was calculated.

3.5 Other research tools

The EMAC (ECHAM/MESSy Atmospheric Chemistry) model comprises the 5th generation of the European Center HAMburg (ECHAM5; Roeckner et al., 2006; version 5.3.01) general circulation model and the Modular Earth Submodel System (MESSy; Jöckel et al., 2016; version 2.52, http://www.messy-interface.org/). Detailed specifications and results have been published previously (Lelieveld et al., 2018).

Ten days back-trajectories were calculated along the flight path using FLEXPART to identify the air mass origin (Tomsche et al., 2019). As indicated by Tomsche et al. prominent source regions of AMA air masses are identified to be the Indo Gangetic Plain, Northeast India, Bangladesh and the Bay of Bengal. Additionally, Tomsche et al. used observations of methane to differentiate between air masses influenced by the south Asian summer monsoon and background air. A comparison of vertical profiles indicated that the air inside the AMA showed significantly higher CH_4 concentrations than

https://doi.org/10.5194/acp-2020-93
Preprint. Discussion started: 19 February 2020


Atmospheric Chemistry and Physics Discussions

outside. Thus, a threshold of $CH_4 \geq 1879.8$ ppb_v was determined to identify monsoon influenced air masses (Tomsche et al., 2019).

4 Results and discussion

4.1 Data processing

Data were averaged to 60 seconds means in order to get the same time resolution for all compounds. The given time is the middle of the block mean. The CH_4 threshold was used to distinguish between air masses influenced by the monsoon ($CH_4 \geq 1879.8$ ppb_v), the SH background ($CH_4 < 1820$ ppb_v) and the NH background (1820 $ppb_v \leq CH_4 < 1879.8$ ppb_v) (Tomsche et al., 2019).

For the histograms the concentrations were binned into samples with a width of 10 ppt_v, starting the plots with the lowest bin. To compare measured and PSS calculated data with the simulations from EMAC, model data were interpolated in time and space onto the flight track in the UT.

4.2 Case study: flight 17

In a case study analyzing flight 17, the method used to determine the origin of the measured air masses and a quantification and comparison of measured and simulated mixing ratios of H_2O_2, MHP and UHP is presented. During this flight we encountered the SH and NH as well as the monsoon in the UT. The flight track is shown in Figure 2 (dotted line). Take-off was in Gan (Maldives) and landing in Bahrain on the Arabian Peninsula. Besides take-off and landing, the entire flight took place in the UT (<230 hPa). The calculated back trajectories show the origin of the air masses. At the beginning of the flight the measured air masses had their origin over the Indian Ocean and Indonesia. During the remaining flight the measured air stemmed from India. Tomsche et al. showed that the measured air in the AMA was affected by deep convection over India resulting in methane mixing ratios above the threshold (Tomsche et al., 2019). Figure 3 shows the time series for measured H_2O_2 during the flight on 10th of August at the time steps given from EMAC (orange circles). The colored bar on top shows the origin of air masses, i.e. red for monsoon, green for NH and blue for SH. The H_2O_2 mixing ratios vary between 128–366 ppt_v. The modelled EMAC H_2O_2 data are in the range of 110–799 ppt_v (grey triangles). For the beginning of the flight model simulations agree rather well with the measurement data. At around 6:00 UTC the model calculated mixing ratios increase to more than 500 ppt_v, while the measured data decrease to 200 ppt_v and lower. In this period a maximum difference between model and *in situ* data of 386 ppt_v was found. One hour later the model data decrease to 416 ppt_v and the *in situ* data increase to 214 ppt_v. During the following hour until around 8:00 UTC both mixing ratios increase with the modelled data showing a much stronger increase up to approximately 800 ppt_v while the *in situ* data increase only to 230 ppt_v. During the last period of the flight, simulated and measured data are again in good agreement. Here the mixing ratios from EMAC are in the range of 110–157 ppt_v while the measured data are in the range of 128–203 ppt_v. This steep drop of the modelled H_2O_2

https://doi.org/10.5194/acp-2020-93
Preprint. Discussion started: 19 February 2020


Atmospheric Chemistry and Physics Discussions

might arise due to a change in the flight altitude, since between 8:01–8:06 UTC the aircraft changed from a flight level at 11,700 m to one aloft at 13,900 m.

In addition to EMAC simulations Figure 3 also shows the calculated PSS-H_2O_2 obtained from equation 15. Observed and PSS values for H_2O_2 mixing ratios agree very well, with a median deviation of 42 ppt_v, well within the combined uncertainties of measured data (25%) and PSS simulations (45%).

In Figure 4 the time series of H_2O_2, MHP and UHP mixing ratios are shown (5 min means). In the beginning of the flight MHP is the dominant organic hydroperoxide. The mixing ratios are in the range of 140–341 ppt_v similar to those of H_2O_2 (143–337 ppt_v). UHP mixing ratios are in the range of 24–162 ppt_v with a mean of 89 ppt_v. Later during the flight UHPs are the dominant hydroperoxides in air masses inside the AMA originating from India. Here we found UHP mixing ratios up to 275 ppt_v. The H_2O_2 mixing ratios show a similar temporal evolution and mixing ratio levels to those of UHP over the Arabian Sea and the Arabian Peninsula, with values in the range of 140–243 ppt_v. MHP mixing ratios are much lower (62–130 ppt_v, median 72 ppt_v) in this area. During this part of the flight the similarity in the time series of acetone and UHP (Figure 5), indicate either similar source regions for both species, or the role of acetone as a precursor for the UHP in monsoon influenced air masses. From 6:20 UTC onwards an increase in both compounds is observed until 7:45 UTC, followed by a steep drop with a minimum at 8:17 UTC. The UHP and acetone mixing ratios in this part of the flight are strongly correlated (Figure 6), with a slope of 0.19±0.02 (ppb_v/ppb_v) and an offset of (-0.003±0.02) ppb_v. The regression coefficient R^2 is very high (0.99). The relation between UHP mixing ratios and an air mass age tracer based on the ratio between [NO] to [NO_y] shows higher values of UHP at smaller ratios representing older or more processed air masses (Figure 7), since highest UHP mixing ratios (>200 ppt_v) are found at the lowest [NO]/[NO_y] ratios (all <0.19). Thus, most of the observed UHP was measured in aged air masses transported within the anticyclone.

4.3 Results for the entire campaign

To extend the analysis to the entire campaign, Figure 8 shows all flight tracks in the UT during OMO. The color-code represents observed mixing ratios of H_2O_2, MHP and UHP varying from low (purple) to high values (red). Histograms for the whole campaign of observed H_2O_2 mixing ratios as well inferred MHP and UHP mixing ratios are presented in Figure 9. Here only data from the UT (<300 hPa which corresponds to altitudes >9 km) were included in the analysis. Mixing ratios for all species were further differentiated by methane levels, such that data in air masses with CH_4 mixing ratios above the threshold of 1879.8 ppb_v were classified as monsoon influenced, while air masses with a CH_4 mixing ratios between 1820 ppb_v and 1879.8 ppb_v were classified as NH background and those with CH_4 <1820 ppb_v as SH following Tomsche et al. (2019). The upper panel indicates that H_2O_2 mixing ratios are most abundant at values of 70–90 ppt_v in NH background air masses (green), 130 ppt_v to 270 ppt_v with three notable peaks at 180–190 ppt_v, 210–220 ppt_v and 250–270 ppt_v in SH air masses (blue) and 150–170 ppt_v in AMA influenced air masses (red). The medians are 115 ppt_v for the NH background, 211 ppt_v for the SH and 167 ppt_v for the AMA, indicating an excess of 52 ppt_v in monsoon influenced air masses compared to the NH background, while in the SH the H_2O_2 mixing ratio is twice as high as the NH background. For MHP (Figure 9,

https://doi.org/10.5194/acp-2020-93
Preprint. Discussion started: 19 February 2020


Atmospheric Chemistry and Physics Discussions

middle panel) the frequency distribution in the NH background shows a maximum at 30–40 ppt_v (green). For AMA influenced air a sharp maximum at 50–70 ppt_v (red) is found, air masses from the SH exhibit a rather flat distribution with a maximum at values of 40–50 ppt_v and a median of 152 ppt_v (blue). With median mixing ratios of 70 ppt_v and 64 ppt_v we found only slightly higher mixing ratios for monsoon influenced air masses in comparison to the NH background. For UHP (Figure 9, bottom panel) we again found a flat distribution of mixing ratios in the SH (blue) with a maximum at values of 140–150 ppt_v and a median of 129 ppt_v. The maximum in the frequency distribution for NH background conditions is found at 70–90 ppt_v (green), while in monsoon influenced air masses it was significantly higher with 210–230 ppt_v (red). Thus, mixing ratios of UHP are approximately 2–3 times higher in the monsoon outflow than in the NH background. This is also represented in the medians of 210 ppt_v in the monsoon and 89 ppt_v in the NH background.

In the analysis of flight 17 we found a strong correlation between UHP and acetone (Figure 6) and an increase of UHP at the highest air mass ages, represented by low [NO]/[NOy] (Figure 7). Extension of this analysis to all observations in the upper troposphere obtained during OMO yields similar results for the relation between UHP and acetone (Figure 10). Enhanced mixing ratios of UHP are typically associated with enhanced acetone mixing ratios. The scatter plot of UHP vs. [NO]/[NOy] for the whole data set, shows no clear correlation with a large spread of UHP mixing ratios at the lowest [NO]/[NO_y] ratios, representing the oldest, i.e. chemically most processed air masses (Figure 11).

4.3.1 H_2O_2 steady-state calculation

A scatter plot of the results from the H_2O_2 steady-state calculation based on observed HO_x data in the UT (eq. 15) is shown in Figure 12. The black dotted line shows the 1:1 line, the green dashed lines represent the 2:1 and 1:2 relations. It is obvious that the comparison is affected by a rather large offset of approximately 350 ppt_v in the observations that is not accounted for in the steady-state calculations. The deviations from unity in the slope are within the combined uncertainties of measured and steady-state estimations of H_2O_2 (51%, 1 σ). The regression coefficient is quite high (0.83), even though most of the calculated steady-state mixing ratios (75%) are in the range between 0 and 65 ppt_v with a median value of 15 ppt_v, while the measured mixing ratios extend over a larger range between 50–203 ppt_v with a median of 150 ppt_v and thus 10 times higher than for steady-state, which can also be seen in the histograms in Figure 13.

4.3.2 Comparison to EMAC

Figure 14 shows histograms for the comparison between H_2O_2, MHP and UHP observations with EMAC simulations. Hydrogen peroxide simulations from EMAC cover a broader range of mixing ratios for both NH background (10 ppt_v up to 580 ppt_v) and AMA (10–720 ppt_v) compared to observations (NH background: 20–310 ppt_v; AMA 40–450 ppt_v). For the SH model simulations and observations cover almost identical ranges of 10–410 ppt_v and 80–510 ppt_v, respectively. Median H_2O_2 values in the model simulations are similar for NH background (66 ppt_v) and AMA (71 ppt_v) conditions (Table 1), while observations indicate an enhancement of +52 ppt_v in the AMA relative to the NH background. For the SH the model

https://doi.org/10.5194/acp-2020-93
Preprint. Discussion started: 19 February 2020


Atmospheric Chemistry and Physics Discussions

simulated H_2O_2 concentration is four times higher than in the NH background (272 ppt_v), while the observations only show a median increase by 96 ppt_v to 211 ppt_v (Table 1).

EMAC simulates MHP mixing ratios in the range of 0–410 ppt_v for background and 0–220 ppt_v within the AMA, similar to the observations with 30–230 ppt_v for the AMA and slightly lower values for the NH background (LOD–210 ppt_v). Again the model simulates highest MHP mixing ratios in the SH with values up to 510 ppt_v compared to up to 350 ppt_v in the observations. Similar as for H_2O_2, medians of MHP for NH background and monsoon conditions are almost identical (11 ppt_v and 13 ppt_v respectively, Table 1) in the model simulations, while the observations show a small difference towards higher mixing ratios in the AMA (64 ppt_v and 70 ppt_v, respectively). In the simulations, southern hemispheric MHP mixing ratios are almost ten times higher than NH background values, compared to two to three times higher in the observations.

Data for UHP in the model are calculated from the sum of simulated ethyl hydroperoxide (EHP) and peroxyacetic acid (PAA), which are the non-methyl organic hydroperoxides in the free troposphere according to the model. UHP mixing ratios in the simulations range from 0–110 ppt_v in the NH background, 0–70 ppt_v in the AMA and 0–100 ppt_v in the SH. UHP based on the observations indicate lowest mixing ratios in the NH background (LOD–260 ppt_v), while in the AMA and the SH the ranges are quite similar (70–320 ppt_v and LOD–340 ppt_v). A comparison of median values emphasizes the large difference between model simulations and observation based estimates. In the NH background, the median UHP mixing ratio from the observations is 81 ppt_v higher than EMAC simulations (89 ppt_v and 8 ppt_v respectively). In the AMA the difference is even larger, with about 200 ppt_v higher UHP levels in the observations compared to the EMAC simulations. The smallest difference with a factor of four was found for the SH (Table 1).

4.3.3 Longitudinal gradients

So far discussions of different air masses have been based on measurements of methane, subdividing the observations in NH background, AMA and SH data. Tomsche et al. (2019) have shown that longitudinal gradients are found in the AMA over the Arabian Peninsula. Observations in the west are often near the edge of the anticyclone, while observations towards the east are closer to its center. In Figure 16 observations, steady-state calculations and EMAC simulations for upper tropospheric (9–15 km) H_2O_2 are displayed as a function of longitude from west to east (20–30 °N, 36–60 °O, according to Figure 15). To identify gradients, the data are subdivided into bins of 2° longitude. The observations (yellow) show roughly a 100% increase of H_2O_2 from west to east (90 ppt_v to 175 ppt_v), similar to simulation with EMAC (black), although absolute mixing ratio levels in EMAC are smaller (61 ppt_v to 121 ppt_v). Contrary to these observed gradients, steady-state calculations of H_2O_2 based on HORUS data (blue) do not vary with longitude, except for the last two bins. The steady-state calculations are based exclusively on observed concentrations of HO_2 and OH radicals and thus yield only the net photochemical production, while the EMAC simulations and the observations will also account for vertical and horizontal advection from up-wind source regions. Bozem et al. (2017) have shown that deep convection can be a source of H_2O_2 in the upper troposphere. Similarly, convection over India during the summer monsoon is a potential source of excess H_2O_2 in the upper

https://doi.org/10.5194/acp-2020-93
Preprint. Discussion started: 19 February 2020


Atmospheric Chemistry and Physics Discussions

troposphere. With a photochemical lifetime of several days, this excess in H_2O_2 reaches the western AMA, giving rise to the observed and model simulated longitudinal gradients. Since the steady-state calculations do not account for transport this can explain the rather large deviation of 150 ppt_v with the observations. Differences between observation and EMAC simulation could potentially arise due to uncertainties in the scavenging efficiency for H_2O_2, as the chemistry does not seem to be a dominant cause of uncertainty.

Similar longitudinal gradients are also observed for measured total organic hydroperoxides (ROOH, green asterisks in Figure 17), inferred UHP (black) as well as total ROOH in EMAC (blue). Steady-state calculations of MHP (pink) and EMAC simulations of MHP (yellow) show either no, or only weak longitudinal gradients. Assuming that MHP is also enhanced in the outflow of deep convection at least part of the enhancement in ROOH (and thus inferred UHP) could be due to advected MHP.

4.4 Discussion

To our knowledge we present the first observations of H_2O_2 and ROOH mixing ratios in the Asian Monsoon Anticyclone. Previous studies have been mainly focused on the northern hemispheric upper troposphere. Several aircraft campaigns including peroxide measurements were performed over North America. They are summarized in Snow et al. (2007): The SONEX campaign took place in fall 1997 in the UT and yielded mean values of 120 ppt_v for H_2O_2 and 50 ppt_v for MHP (medians: 80 ppt_v and 30 ppt_v, respectively). The TOPSE campaign in winter/spring 2000 probed the middle troposphere yielding median H_2O_2 and MHP mixing ratios of 150 ppt_v for both species. During the INTEX-NA campaign in summer 2004 observed median mixing ratios at altitudes of 6–10 km were about 400 ppt_v for H_2O_2, and 200 ppt_v for MHP. A comparison with our results (Table 1) shows that we found similar mixing ratios as in SONEX in the northern hemispheric background of 115 ppt_v and 64 ppt_v for H_2O_2 and MHP, respectively. Mixing ratios for both species reported for TOPSE and INTEX-NA are slightly higher than ours, which may be related to the lower altitude range of 6–10 km (in comparison to >9 km for OMO) in these studies. Previous observations have shown that H_2O_2 and MHP show highest mixing ratios at altitudes between 2–5 km followed by a sharp decrease towards higher altitudes (see e.g. Daum et al., 1990; Heikes, 1992; Weinstein-Lloyd et al., 1998; Snow, 2003; Snow et al., 2007; Klippel et al., 2011).

Heikes et al. associated enhanced H_2O_2 mixing ratios above 5 km in the North Pacific of the Asian coast (30 °N) with outflow from the typhoon Mireille (Heikes et al., 1996). These observations were made close to the source region for the monsoon influenced air masses described here (see back trajectories in the case study of flight 17, Figure 2 or Tomsche et al., 2019). For MHP Heikes et al. (1996) found mixing ratios of 250–500 ppt_v in the southern longitudinal section above 5 km, similar to median mixing ratios of 152 ppt_v for MHP in SH air masses in the UT found in this study.

Although the mixing ratios observed during this study are similar to previous observations in the upper troposphere, one striking result is that a state-of-the-art global circulation model (EMAC) and a local steady-state calculation constrained by measured radical levels significantly underestimate H_2O_2 mixing ratios in particular in the AMA. The general tendency is that the steady-state model produces the lowest values, with EMAC falling in between steady-state and observations (e.g.

https://doi.org/10.5194/acp-2020-93
Preprint. Discussion started: 19 February 2020


Atmospheric Chemistry and Physics Discussions

Figure 16). A comparison of the EMAC simulations for the two radicals that affect H_2O_2 most strongly (OH and HO_2) yields a rather good agreement. A scatter plot between modelled and observed HO_2 yields a slope of 0.72±0.01 (ppt_v/ppt_v) and an offset of (4.30±0.09) ppt_v with a regression coefficient R^2 of 0.89 (Figure 18 left). The OH data show more scatter with a tendency for EMAC to overestimate the mixing ratios (slope: 1.7±0.2 (ppt_v/ppt_v); offset: (-0.1±0.1) ppt_v; regression coefficient: 0.67, Figure 18 right). Although there is rather good agreement between EMAC simulations and observations for all the species that affect the local photochemical budget of H_2O_2, EMAC significantly exceeds PSS calculation for H_2O_2. This is an indication that an additional H_2O_2 source is accounted for in the model and that the local photo-stationary-state assumption is not fulfilled. The additional source is attributed to transport associated with deep convection over India, yielding in an upwind source of H_2O_2 that is significant throughout the western part of the AMA. In the AMA, clouds are absent, so that gas phase photochemical processes may determine the lifetime of H_2O_2. Based on observed OH levels and photolysis frequencies during OMO the H_2O_2 lifetime in the upper troposphere is of the order of several days, sufficiently long for the excess H_2O_2 to reach the western parts of the AMA, producing the observed longitudinal H_2O_2 gradient observed in both observations and EMAC simulations (Figure 16). The total amount of H_2O_2 injected into the UT by convective outflow depends on the scavenging efficiency (Mari et al., 2000; Barth et al., 2016; Bozem et al., 2017). Differences between H_2O_2 observations and EMAC simulations are most likely due to an overestimation of scavenging in the model as also pointed out by Klippel et al. (2011). To investigate this assumption we performed a sensitivity study with EMAC excluding scavenging. The result is shown in Figure 19. The H_2O_2 mixing ratios significantly increase with longitude by a factor of 3–4 and thus to the level of observed H_2O_2.

There is a rather large uncertainty regarding the scavenging efficiency of MHP in deep convection (Barth et al., 2016). For the Trace A campaign Mari et al. (2000) found observed (modelled) enhancement ratios of postconvective to preconvective mixing ratios of 11 (9.5) for MHP and 1.9 (1.2) for H_2O_2. Such efficient transport in the Indian Summer Monsoon would yield a strong source of upper tropospheric MHP explaining the large enhancement of ROOH in the AMA described here. It seems that a large part of the UHP is actually MHP advected throughout the AMA after deep convective transport over India.

5 Conclusion

Hydrogen peroxide and organic hydroperoxides were measured during the OMO campaign in the upper troposphere in NH background air over the western Mediterranean, the Asian Summer Monsoon Anticyclone over the Arabian Peninsula and the SH over the Maldives and the Indian Ocean in summer 2015. The observed mixing ratios for background conditions in the NH and SH are in line with previous studies described in the literature. A case study (of flight 17) revealed enhanced H_2O_2 and ROOH mixing ratios in the AMA relative to the NH background. Similar results are found for other flights throughout the campaign. The atmospheric chemistry-general circulation model EMAC slightly underestimates H_2O_2 in the NH background, significantly underestimates it in the AMA, and overestimates it in the SH. Steady-state calculations for

https://doi.org/10.5194/acp-2020-93
Preprint. Discussion started: 19 February 2020


Atmospheric Chemistry and Physics Discussions

H_2O_2 and MHP based on observed precursors yield much lower values, in particular in the AMA, resulting in a large contribution of an unidentified organic hydroperoxide (UHP) in air masses affected by the Asian summer monsoon. A comparison between EMAC simulations and HO_x levels shows a good agreement indicating that deviations between simulated and steady-state H_2O_2 levels are due to transport. Convective injection of H_2O_2 (and MHP) into the upper troposphere over India most likely forms a pool of hydroperoxides in the upper troposphere that subsequently influences the western AMA, giving rise to a significant longitudinal gradient of H_2O_2 and MHP mixing ratios, with increasing values towards the center of the AMA. It is likely that at least a large part of UHP is due to additional MHP from an up-wind source.

Data availability

The data are available from the HALO database (https://halo-db.pa.op.dlr.de/, last access: 7 November 2019).

Author contributions

BH and SH were responsible for H_2O_2 and ROOH measurements and data. BH conducted further data analysis and wrote the original draft of the paper in close cooperation with HF. CH_4 and CO data were provided by LT, HO_x data by DM, MM and HH, O_3 and acetone data by MN and AZ, photolysis frequencies by BB and NO and NO_y data by HZ. AP was responsible for the EMAC model simulations. JL was the principal investigator of the OMO mission. All authors were involved in the review and editing of the paper.

Competing interests

The authors declare that they have no conflict of interest.

Acknowledgements

We would like to thank all of the participants of the OMO mission, the German Aerospace Center (DLR), and EDT Offshore Ltd in Cyprus for their cooperation during the mission. We further thank Rainer Königstedt for installing the TRIHOP instrument and Uwe Parchatka for supporting the measurements of CO and CH_4.

https://doi.org/10.5194/acp-2020-93
Preprint. Discussion started: 19 February 2020

Atmospheric Chemistry and Physics Discussions

References

AEROLASER: AL2021 H_2O_2-Monitor User Manual, Version 2.20, Rev.02, Garmisch-Partenkirchen, Germany, 2006.

Atkinson, R., Baulch, D. L., Cox, R. A., Crowley, J. N., Hampson, R. F., Hynes, R. G., Jenkin, M. E., Rossi, M. J., and Troe, J.: Evaluated kinetic and photochemical data for atmospheric chemistry: Volume I – gas phase reactions of O_x, HO_x, NO_x and SO_x species, Atmos. Chem. Phys., 4, 1461–1738, doi:10.5194/acp-4-1461-2004, 2004.

Atkinson, R., Baulch, D. L., Cox, R. A., Crowley, J. N., Hampson, R. F., Hynes, R. G., Jenkin, M. E., Rossi, M. J., Troe, J., and IUPAC Subcommittee: Evaluated kinetic and photochemical data for atmospheric chemistry: Volume II – gas phase reactions of organic species, Atmos. Chem. Phys., 6, 3625–4055, doi:10.5194/acp-6-3625-2006, 2006.

Barret, B., Sauvage, B., Bennouna, Y., and Le Flochmoen, E.: Upper-tropospheric CO and O_3 budget during the Asian summer monsoon, Atmos. Chem. Phys., 16, 9129–9147, doi:10.5194/acp-16-9129-2016, 2016.

Barth, M. C., Bela, M. M., Fried, A., Wennberg, P. O., Crounse, J. D., St. Clair, J. M., Blake, N. J., Blake, D. R., Homeyer, C. R., Brune, W. H., Zhang, L., Mao, J., Ren, X., Ryerson, T. B., Pollack, I. B., Peischl, J., Cohen, R. C., Nault, B. A., Huey, L. G., Liu, X., and Cantrell, C. A.: Convective transport and scavenging of peroxides by thunderstorms observed over the central U.S. during DC3, J. Geophys. Res. Atmos., 121, 4272–4295, doi:10.1002/2015JD024570, 2016.

Bohn, B. and Lohse, I.: Calibration and evaluation of CCD spectroradiometers for ground-based and airborne measurements of spectral actinic flux densities, Atmos. Meas. Tech., 10, 3151–3174, doi:10.5194/amt-10-3151-2017, 2017.

Bozem, H., Pozzer, A., Harder, H., Martinez, M., Williams, J., Lelieveld, J., and Fischer, H.: The influence of deep convection on HCHO and H_2O_2 in the upper troposphere over Europe, Atmos. Chem. Phys., 17, 11835–11848, doi:10.5194/acp-17-11835-2017, 2017.

Burkholder, J. B., Sander S. P., Abbatt J., Barker J. R., Huie R. E., Kolb C. E., Kurylo M. J., Orkin V. L., and Wilmouth D. M. and Wine P. H.: Chemical Kinetics and Photochemical Data for Use in Atmospheric Studies, JPL Publication 15-10, Jet Propulsion Laboratory, Pasadena, 2015.

Calvert, J. G., Lazrus, A., Kok, G. L., Heikes, B. G., Walega, J. G., Lind, J., and Cantrell, C. A.: Chemical mechanisms of acid generation in the troposphere, Nature, 317, 27–35, doi:10.1038/317027a0, 1985.

Crutzen, P. J., Lawrence, M. G., and Pöschl, U.: On the background photochemistry of tropospheric ozone, Tellus B: Chemical and Physical Meteorology, 51, 123–146, doi:10.3402/tellusb.v51i1.16264, 1999.

Daum, P. H., Kleinman, L. I., Hills, A. J., Lazrus, A. L., Leslie, A. C. D., Busness, K., and Boatman, J.: Measurement and interpretation of concentrations of H_2O_2 and related species in the upper midwest during summer, J. Geophys. Res., 95, 9857–9871, doi:10.1029/JD095iD07p09857, 1990.

Faloona, I., Tan, D., Brune, W. H., Jaeglé, L., Jacob, D. J., Kondo, Y., Koike, M., Chatfield, R., Pueschel, R., Ferry, G., Sachse, G., Vay, S., Anderson, B., Hannon, J., and Fuelberg, H.: Observations of HO_x and its relationship with NO_x in the upper troposphere during SONEX, J. Geophys. Res., 105, 3771–3783, doi:10.1029/1999JD900914, 2000.

505 Faloona, I. C., Tan, D., Lesher, R. L., Hazen, N. L., Frame, C. L., Simpas, J. B., Harder, H., Martinez, M., Di Carlo, P., Ren, X., and Brune, W. H.: A Laser-induced Fluorescence Instrument for Detecting Tropospheric OH and HO_2: Characteristics and Calibration, Journal of Atmospheric Chemistry, 47, 139–167, doi:10.1023/B:JOCH.0000021036.53185.0e, 2004.

Gettelman, A., Kinnison, D. E., Dunkerton, T. J., and Brasseur, G. P.: Impact of monsoon circulations on the upper
510 troposphere and lower stratosphere, J. Geophys. Res., 109, n/a-n/a, doi:10.1029/2004JD004878, 2004.

Heikes, B. G.: Formaldehyde and hydroperoxides at Mauna Loa Observatory, J. Geophys. Res., 97, 18001, doi:10.1029/92JD00268, 1992.

Heikes, B. G., Lee, M., Bradshaw, J., Sandholm, S., Davis, D. D., Crawford, J., Rodriguez, J., Liu, S., McKeen, S., Thornton, D., Bandy, A., Gregory, G., Talbot, R., and Blake, D.: Hydrogen peroxide and methylhydroperoxide
515 distributions related to ozone and odd hydrogen over the North Pacific in the fall of 1991, J. Geophys. Res., 101, 1891–1905, doi:10.1029/95JD01364, 1996.

Hoffmann, M. R. and Edwards, J. O.: Kinetics of the oxidation of sulfite by hydrogen peroxide in acidic solution, J. Phys. Chem., 79, 2096–2098, doi:10.1021/j100587a005, 1975.

Jackson, A. V. and Hewitt, C. N.: Hydrogen peroxide and organic hydroperoxide concentrations in air in a eucalyptus forest
520 in central Portugal, Atmospheric Environment, 30, 819–830, doi:10.1016/1352-2310(95)00348-7, 1996.

Jacob, P. and Klockow, D.: Hydrogen peroxide measurements in the marine atmosphere, J Atmos Chem, 15, 353–360, doi:10.1007/BF00115404, 1992.

Jaeglé, L., Jacob, D. J., Brune, W. H., Faloona, I., Tan, D., Heikes, B. G., Kondo, Y., Sachse, G. W., Anderson, B., Gregory, G. L., Singh, H. B., Pueschel, R., Ferry, G., Blake, D. R., and Shetter, R. E.: Photochemistry of HO_x in the upper
525 troposphere at northern midlatitudes, J. Geophys. Res., 105, 3877–3892, doi:10.1029/1999JD901016, 2000.

Jaeglé, L., Jacob, D. J., Wennberg, P. O., Spivakovsky, C. M., Hanisco, T. F., Lanzendorf, E. J., Hintsa, E. J., Fahey, D. W., Keim, E. R., Proffitt, M. H., Atlas, E. L., Flocke, F., Schauffler, S., McElroy, C. T., Midwinter, C., Pfister, L., and Wilson, J. C.: Observed OH and HO_2 in the upper troposphere suggest a major source from convective injection of peroxides, Geophys. Res. Lett., 24, 3181–3184, doi:10.1029/97GL03004, 1997.

530 Jöckel, P., Tost, H., Pozzer, A., Kunze, M., Kirner, O., Brenninkmeijer, C. A. M., Brinkop, S., Cai, D. S., Dyroff, C., Eckstein, J., Frank, F., Garny, H., Gottschaldt, K.-D., Graf, P., Grewe, V., Kerkweg, A., Kern, B., Matthes, S., Mertens, M., Meul, S., Neumaier, M., Nützel, M., Oberländer-Hayn, S., Ruhnke, R., Runde, T., Sander, R., Scharffe, D., and Zahn, A.: Earth System Chemistry integrated Modelling (ESCiMo) with the Modular Earth Submodel System (MESSy) version 2.51, Geosci. Model Dev., 9, 1153–1200, doi:10.5194/gmd-9-1153-2016, 2016.

535 Klippel, T., Fischer, H., Bozem, H., Lawrence, M. G., Butler, T., Jöckel, P., Tost, H., Martinez, M., Harder, H., Regelin, E., Sander, R., Schiller, C. L., Stickler, A., and Lelieveld, J.: Distribution of hydrogen peroxide and formaldehyde over Central Europe during the HOOVER project, Atmos. Chem. Phys., 11, 4391–4410, doi:10.5194/acp-11-4391-2011, 2011.

Lazrus, A. L., Kok, G. L., Gitlin, S. N., Lind, J. A., and McLaren, S. E.: Automated fluorimetric method for hydrogen peroxide in atmospheric precipitation, Anal. Chem., 57, 917–922, doi:10.1021/ac00281a031, 1985.

Lazrus, A. L., Kok, G. L., Lind, J. A., Gitlin, S. N., Heikes, B. G., and Shetter, R. E.: Automated fluorometric method for hydrogen peroxide in air, Anal. Chem., 58, 594–597, doi:10.1021/ac00294a024, 1986.

Lee, M., Heikes, B. G., and O'Sullivan, D. W.: Hydrogen peroxide and organic hydroperoxide in the troposphere: A review, Atmospheric Environment, 34, 3475–3494, doi:10.1016/S1352-2310(99)00432-X, 2000.

Lelieveld, J., Berresheim, H., Borrmann, S., Crutzen, P. J., Dentener, F. J., Fischer, H., Feichter, J., Flatau, P. J., Heland, J., Holzinger, R., Korrmann, R., Lawrence, M. G., Levin, Z., Markowicz, K. M., Mihalopoulos, N., Minikin, A., Ramanathan, V., Reus, M. de, Roelofs, G. J., Scheeren, H. A., Sciare, J., Schlager, H., Schultz, M., Siegmund, P., Steil, B., Stephanou, E. G., Stier, P., Traub, M., Warneke, C., Williams, J., and Ziereis, H.: Global air pollution crossroads over the Mediterranean, Science (New York, N.Y.), 298, 794–799, doi:10.1126/science.1075457, 2002.

Lelieveld, J., Bourtsoukidis, E., Brühl, C., Fischer, H., Fuchs, H., Harder, H., Hofzumahaus, A., Holland, F., Marno, D., Neumaier, M., Pozzer, A., Schlager, H., Williams, J., Zahn, A., and Ziereis, H.: The South Asian monsoon-pollution pump and purifier, Science (New York, N.Y.), 361, 270–273, doi:10.1126/science.aar2501, 2018.

Lelieveld, J. and Crutzen, P. J.: Influences of cloud photochemical processes on tropospheric ozone, Nature, 343, 227–233, doi:10.1038/343227a0, 1990.

Levy, H.: Normal atmosphere: large radical and formaldehyde concentrations predicted, Science (New York, N.Y.), 173, 141–143, doi:10.1126/science.173.3992.141, 1971.

Lind, J. A. and Kok, G. L.: Henry's law determinations for aqueous solutions of hydrogen peroxide, methylhydroperoxide, and peroxyacetic acid, J. Geophys. Res., 91, 7889–7895, doi:10.1029/JD091iD07p07889, 1986.

Lind, J. A. and Kok, G. L.: Correction to “Henry's law determinations for aqueous solutions of hydrogen peroxide, methylhydroperoxide, and peroxyacetic acid”, J. Geophys. Res., 99, 21119, doi:10.1029/94JD01155, 1994.

Mari, C., Jacob, D. J., and Bechtold, P.: Transport and scavenging of soluble gases in a deep convective cloud, J. Geophys. Res., 105, 22255–22267, doi:10.1029/2000JD900211, 2000.

Martinez, M., Harder, H., Kubistin, D., Rudolf, M., Bozem, H., Eerdekens, G., Fischer, H., Klüpfel, T., Gurk, C., Königstedt, R., Parchatka, U., Schiller, C. L., Stickler, A., Williams, J., and Lelieveld, J.: Hydroxyl radicals in the tropical troposphere over the Suriname rainforest: Airborne measurements, Atmos. Chem. Phys., 10, 3759–3773, doi:10.5194/acp-10-3759-2010, 2010.

Nunnermacker, L. J., Weinstein-Lloyd, J. B., Hillery, B., Giebel, B., Kleinman, L. I., Springston, S. R., Daum, P. H., Gaffney, J., Marley, N., and Huey, G.: Aircraft and ground-based measurements of hydroperoxides during the 2006 MILAGRO field campaign, Atmos. Chem. Phys., 8, 7619–7636, doi:10.5194/acp-8-7619-2008, 2008.

Ojha, N., Pozzer, A., Rauthe-Schöch, A., Baker, A. K., Yoon, J., Brenninkmeijer, C. A. M., and Lelieveld, J.: Ozone and carbon monoxide over India during the summer monsoon: Regional emissions and transport, Atmos. Chem. Phys., 16, 3013–3032, doi:10.5194/acp-16-3013-2016, 2016.

https://doi.org/10.5194/acp-2020-93
Preprint. Discussion started: 19 February 2020


Atmospheric Chemistry and Physics Discussions

Penkett, S. A., Jones, B., Brich, K. A., and Eggleton, A.: The importance of atmospheric ozone and hydrogen peroxide in oxidising sulphur dioxide in cloud and rainwater, Atmospheric Environment (1967), 13, 123–137, doi:10.1016/0004-6981(79)90251-8, 1979.

Perros, P.: Large-scale distribution of hydrogen peroxide from aircraft measurements during the TROPOZ II experiment, Atmospheric Environment. Part A. General Topics, 27, 1695–1708, doi:10.1016/0960-1686(93)90232-N, 1993.

Pilz, W. and Johann, I.: Die Bestimmung Kleinster Mengen von Wasserstoffperoxyd in Luft, International journal of environmental analytical chemistry, 3, 257–270, doi:10.1080/03067317408071087, 1974.

Randel, W. J., Park, M., Emmons, L., Kinnison, D., Bernath, P., Walker, K. A., Boone, C., and Pumphrey, H.: Asian monsoon transport of pollution to the stratosphere, Science (New York, N.Y.), 328, 611–613, doi:10.1126/science.1182274, 2010.

Rauthe-Schöch, A., Baker, A. K., Schuck, T. J., Brenninkmeijer, C. A. M., Zahn, A., Hermann, M., Stratmann, G., Ziereis, H., van Velthoven, Peter F. J., and Lelieveld, J.: Trapping, chemistry, and export of trace gases in the South Asian summer monsoon observed during CARIBIC flights in 2008, Atmos. Chem. Phys., 16, 3609–3629, doi:10.5194/acp-16-3609-2016, 2016.

Robbin Martin, L. and Damschen, D. E.: Aqueous oxidation of sulfur dioxide by hydrogen peroxide at low pH, Atmospheric Environment (1967), 15, 1615–1621, doi:10.1016/0004-6981(81)90146-3, 1981.

Roeckner, E., Brokopf, R., Esch, M., Giorgetta, M., Hagemann, S., Kornblueh, L., Manzini, E., Schlese, U., and Schulzweida, U.: Sensitivity of Simulated Climate to Horizontal and Vertical Resolution in the ECHAM5 Atmosphere Model, J. Climate, 19, 3771–3791, doi:10.1175/JCLI3824.1, 2006.

Schiller, C. L., Bozem, H., Gurk, C., Parchatka, U., Königstedt, R., Harris, G. W., Lelieveld, J., and Fischer, H.: Applications of quantum cascade lasers for sensitive trace gas measurements of CO, CH_4, N_2O and HCHO, Appl. Phys. B, 92, 419–430, doi:10.1007/s00340-008-3125-0, 2008.

Slemr, F. and Tremmel, H. G.: Hydroperoxides in the marine troposphere over the Atlantic Ocean, J Atmos Chem, 19, 371–404, doi:10.1007/BF00694493, 1994.

Snow, J. A.: Winter-spring evolution and variability of HO_x reservoir species, hydrogen peroxide, and methyl hydroperoxide, in the northern middle to high latitudes, J. Geophys. Res., 108, 1890, doi:10.1029/2002JD002172, 2003.

Snow, J. A., Heikes, B. G., Shen, H., O'Sullivan, D. W., Fried, A., and Walega, J.: Hydrogen peroxide, methyl hydroperoxide, and formaldehyde over North America and the North Atlantic, J. Geophys. Res., 112, 8353, doi:10.1029/2006JD007746, 2007.

Stratmann, G., Ziereis, H., Stock, P., Brenninkmeijer, C., Zahn, A., Rauthe-Schöch, A., Velthoven, P. V., Schlager, H., and Volz-Thomas, A.: NO and NO_y in the upper troposphere: Nine years of CARIBIC measurements onboard a passenger aircraft, Atmospheric Environment, 133, 93–111, doi:10.1016/j.atmosenv.2016.02.035, 2016.

https://doi.org/10.5194/acp-2020-93
Preprint. Discussion started: 19 February 2020

Atmospheric Chemistry and Physics Discussions

605 Tadic, I., Parchatka, U., Königstedt, R., and Fischer, H.: In-flight stability of quantum cascade laser-based infrared absorption spectroscopy measurements of atmospheric carbon monoxide, Appl. Phys. B, 123, 805, doi:10.1007/s00340-017-6721-z, 2017.

Tomsche, L., Pozzer, A., Ojha, N., Parchatka, U., Lelieveld, J., and Fischer, H.: Upper tropospheric CH_4 and CO affected by the South Asian summer monsoon during the Oxidation Mechanism Observations mission, Atmos. Chem. Phys., 19,
610 1915–1939, doi:10.5194/acp-19-1915-2019, 2019.

Weinstein-Lloyd, J. B., Lee, J. H., Daum, P. H., Kleinman, L. I., Nunnermacker, L. J., Springston, S. R., and Newman, L.: Measurements of peroxides and related species during the 1995 summer intensive of the Southern Oxidants Study in Nashville, Tennessee, J. Geophys. Res., 103, 22361–22373, doi:10.1029/98JD01636, 1998.

Zahn, A., Weppner, J., Widmann, H., Schlote-Holubek, K., Burger, B., Kühner, T., and Franke, H.: A fast and precise
615 chemiluminescence ozone detector for eddy flux and airborne application, Atmos. Meas. Tech., 5, 363–375, doi:10.5194/amt-5-363-2012, 2012.

Ziereis, H., Schlager, H., Schulte, P., van Velthoven, P. F. J., and Slemr, F.: Distributions of NO, NO_x and NO_y in the upper troposphere and lower stratosphere between 28° and 61°N during POLINAT 2, J. Geophys. Res., 105, 3653–3664, doi:10.1029/1999JD900870, 2000.

620

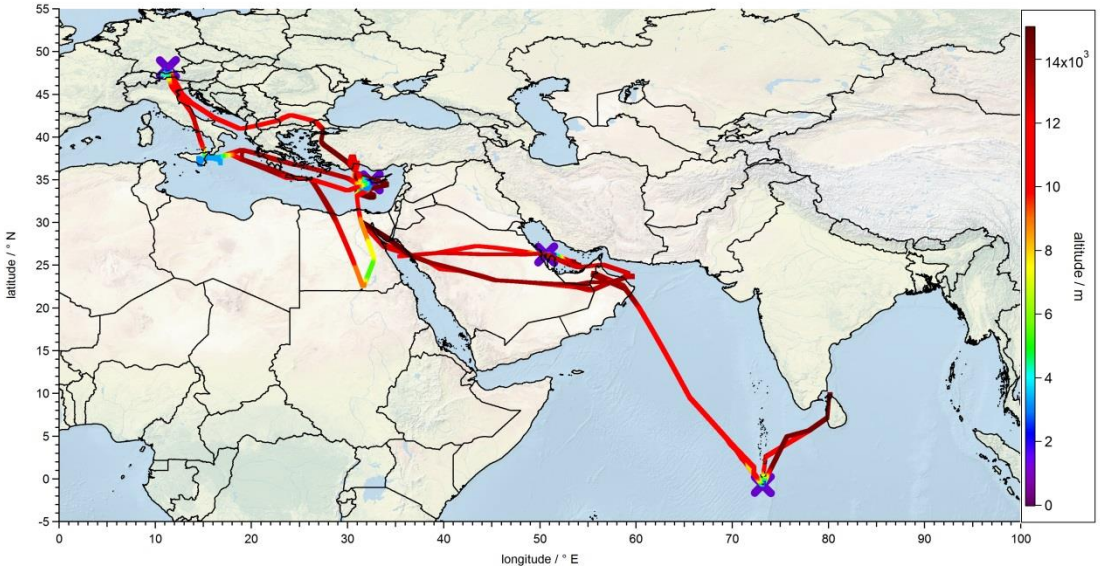

Figure 1: Flight tracks (colors indicate altitude) and airports (purple crosses) used during the OMO campaign.

https://doi.org/10.5194/acp-2020-93
Preprint. Discussion started: 19 February 2020

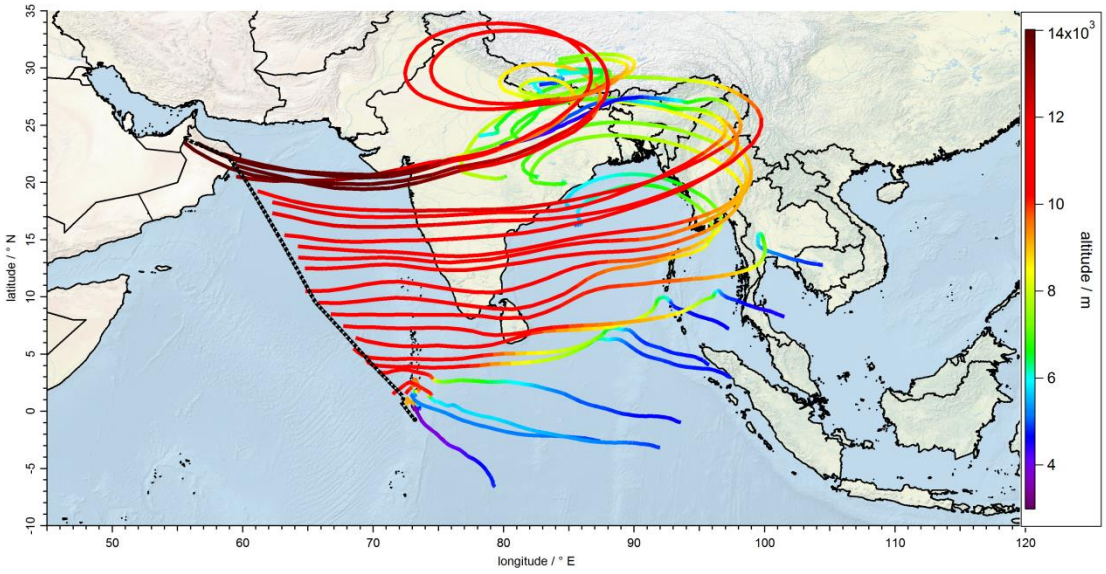

Figure 2: Track of flight 17 (black dotted line) and calculated back trajectories (lines colored as a function of altitude) to show the origin of sampled air masses during the flight.

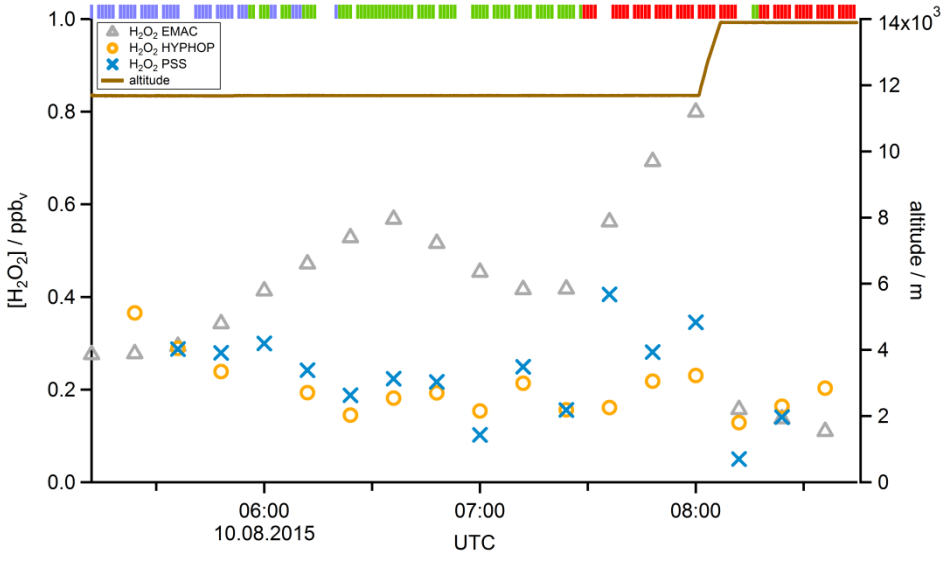

Figure 3: Time series of measured (orange circles), data-constrained calculated (blue crosses) and modelled (grey triangles) H_2O_2 mixing ratios for flight 17. The brown line shows the altitude, the colored bar on top indicates the origin of air masses according to the methane mixing ratio classification: for SH blue, NH green and monsoon red.

https://doi.org/10.5194/acp-2020-93
Preprint. Discussion started: 19 February 2020

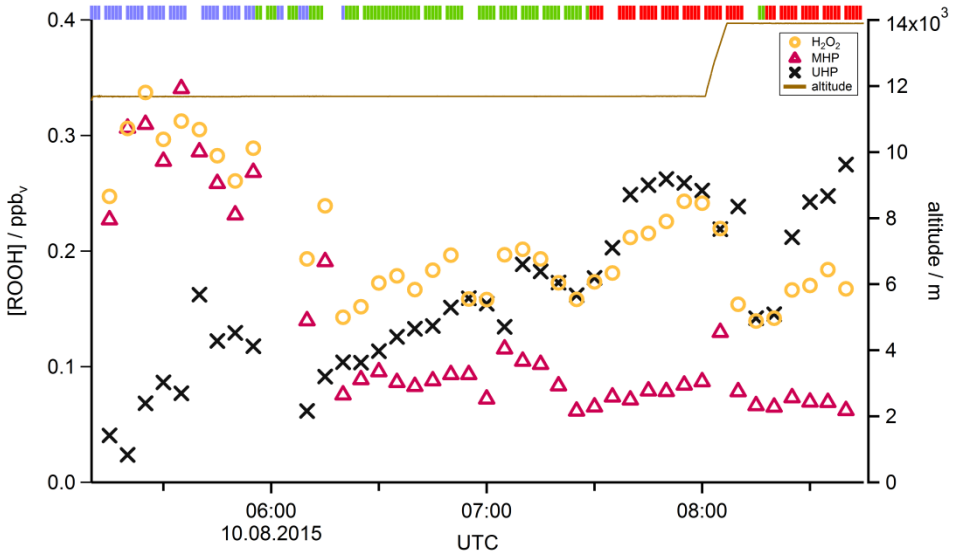

Figure 4: Time series of hydroperoxide mixing ratios during flight 17. The mixing ratios of H_2O_2 (orange circles), MHP (purple triangles) and UHP (black crosses) are shown. The brown line shows the altitude, the colored bar on top indicates the origin of air masses according to the methane mixing ratio classification: for SH blue, NH green and monsoon red.

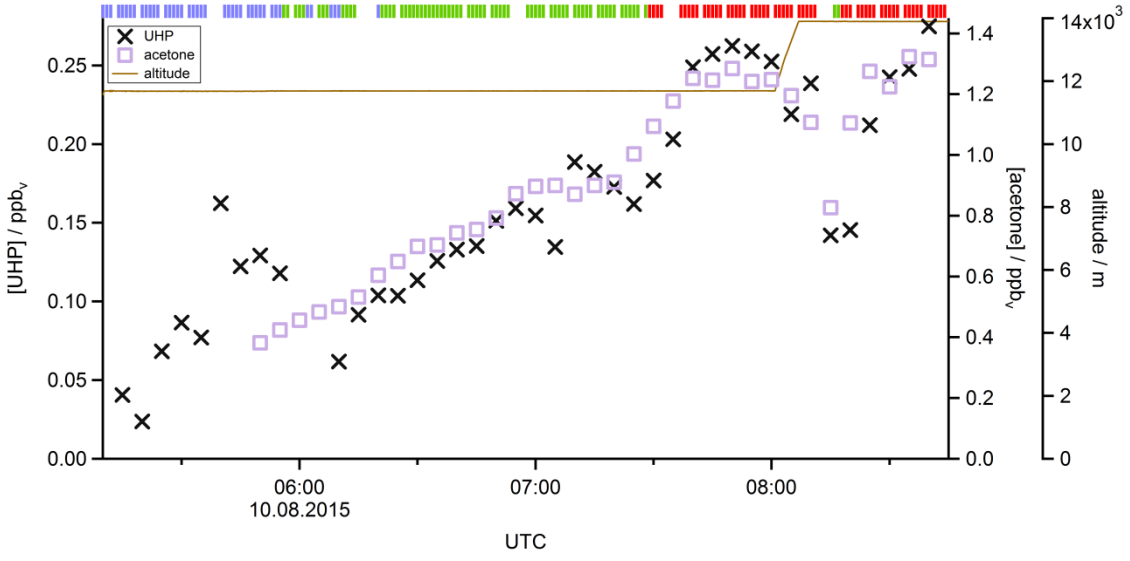

635

Figure 5: Time series of UHP (black crosses) and acetone (green circles) mixing ratios during flight 17. The brown line shows the altitude, the colored bar on top indicates the origin of air masses according to the methane mixing ratio classification: for SH blue, NH green and monsoon red.

https://doi.org/10.5194/acp-2020-93
Preprint. Discussion started: 19 February 2020

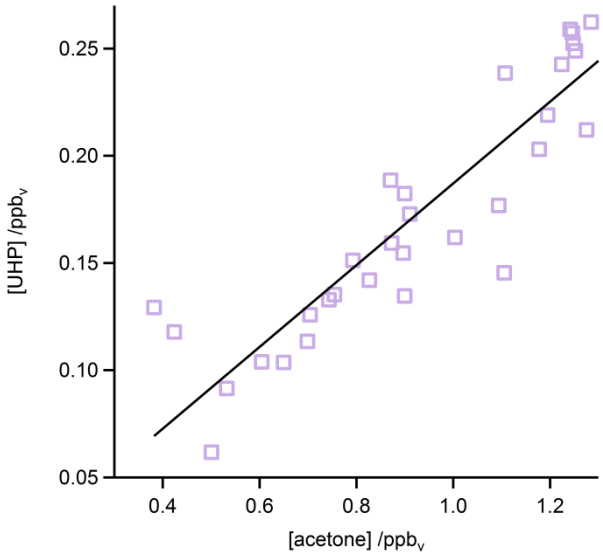

640

Figure 6: Scatter plot of measured acetone and calculated UHP during flight 17. The black line represents the least orthogonal distance fit with a regression coefficient of 0.99.

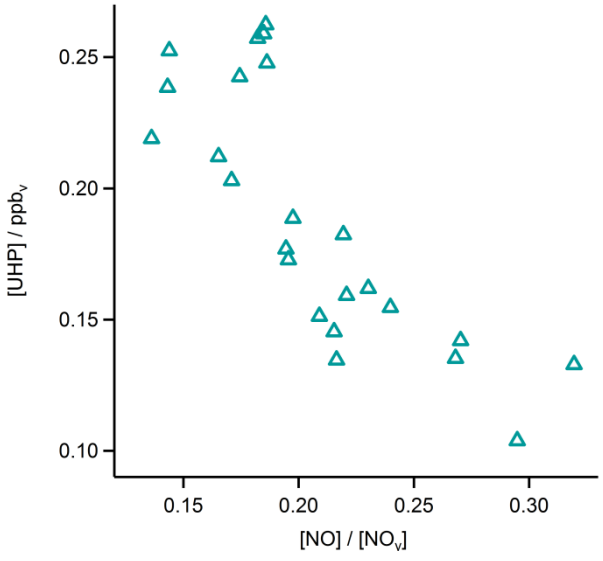

Figure 7: Scatter plot of [UHP] and [NO]/[NO_y] ratio during flight 17.

https://doi.org/10.5194/acp-2020-93
Preprint. Discussion started: 19 February 2020

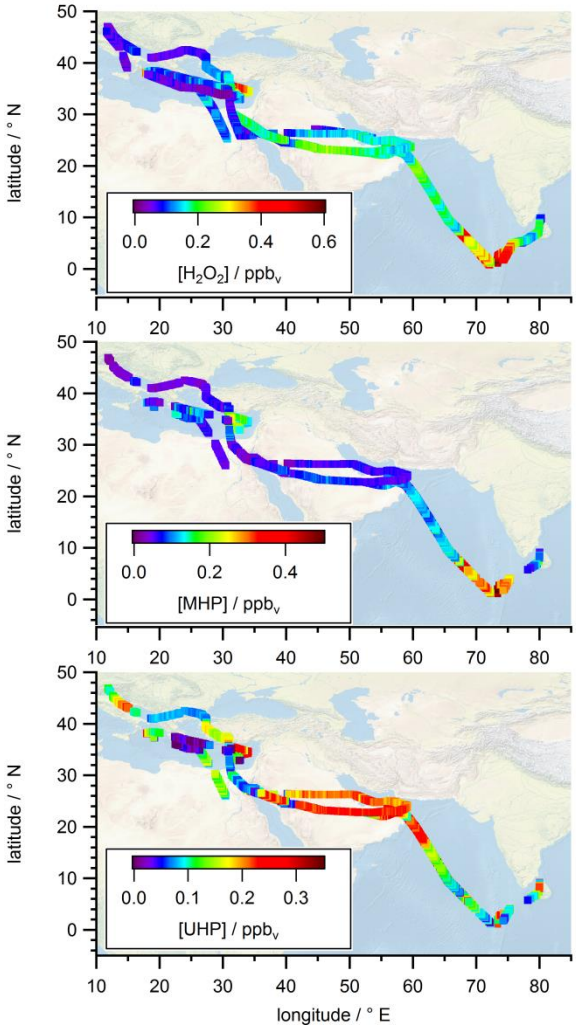

Figure 8: All flight positions in the upper troposphere during OMO as a function of (a) [H_2O_2] on top, (b) [MHP] in the middle and (c) [UHP] at the bottom.

https://doi.org/10.5194/acp-2020-93
Preprint. Discussion started: 19 February 2020

Atmospheric Chemistry and Physics Discussions

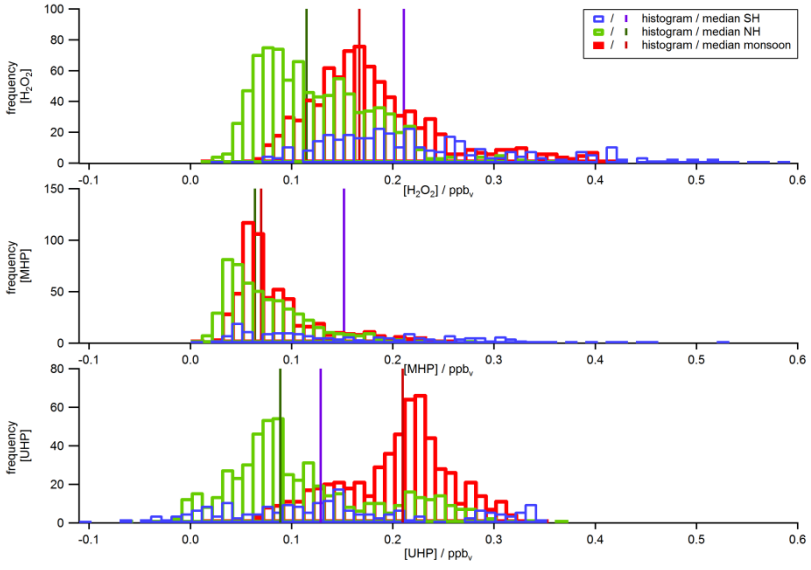

Figure 9: Histograms of H_2O_2 (top), MHP (middle) and UHP (bottom) mixing ratios during the OMO campaign for NH background (green), SH (blue) and monsoon (red) air masses.

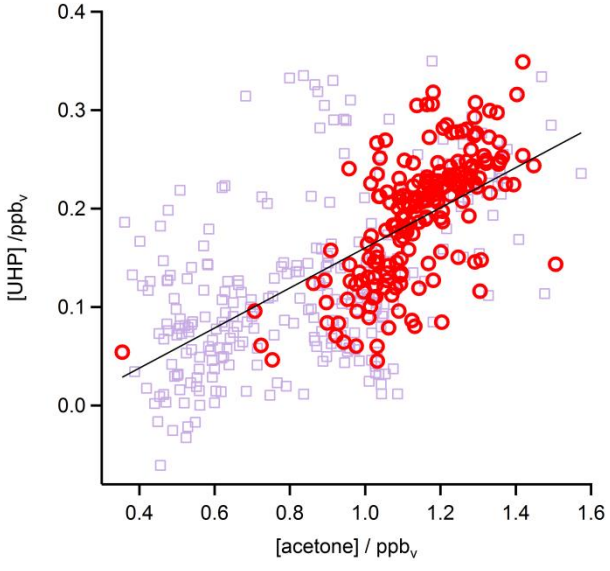

Figure 10: Scatter plot of acetone and UHP in the UT (purple squares) and especially in the AMA (red circles). The black line represents the least orthogonal distance fit with a linear regression coefficient of 0.96.

https://doi.org/10.5194/acp-2020-93
Preprint. Discussion started: 19 February 2020

Atmospheric Chemistry and Physics Discussions

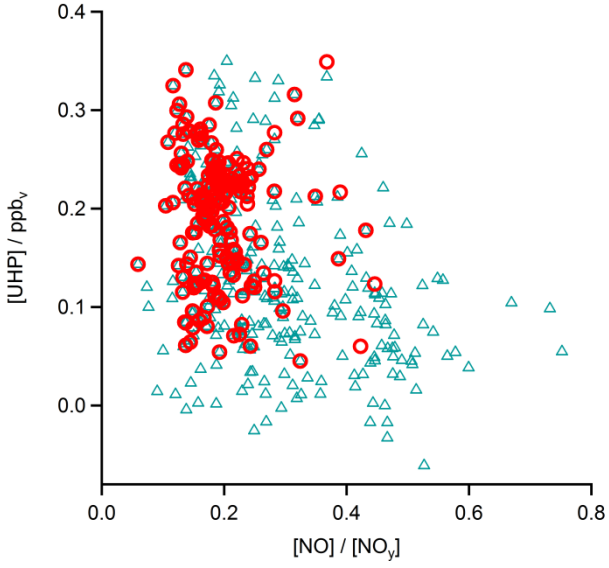

665

Figure 11: Scatter plot of [UHP] and [NO]/[NO_y] in the UT (blue triangles) and especially in the AMA (red circles).

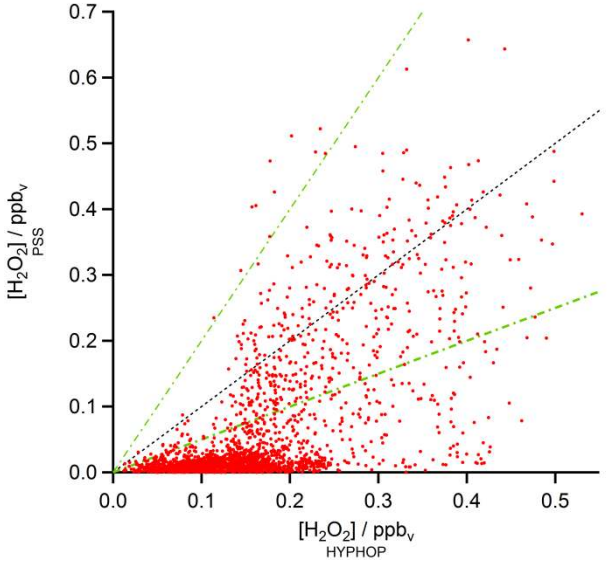

Figure 12: Scatter plot of measured and calculated H_2O_2 mixing ratios (red) with the 1:1 (black), 1:2 and 2:1 (both green) lines.

https://doi.org/10.5194/acp-2020-93
Preprint. Discussion started: 19 February 2020

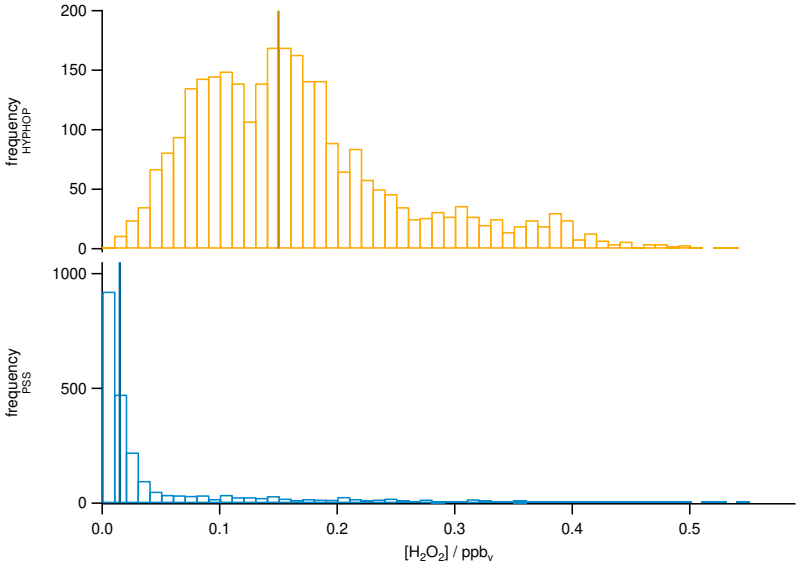

Figure 13: Histograms of measured (top) and calculated (bottom) H_2O_2 mixing ratios and the associated medians.

https://doi.org/10.5194/acp-2020-93
Preprint. Discussion started: 19 February 2020

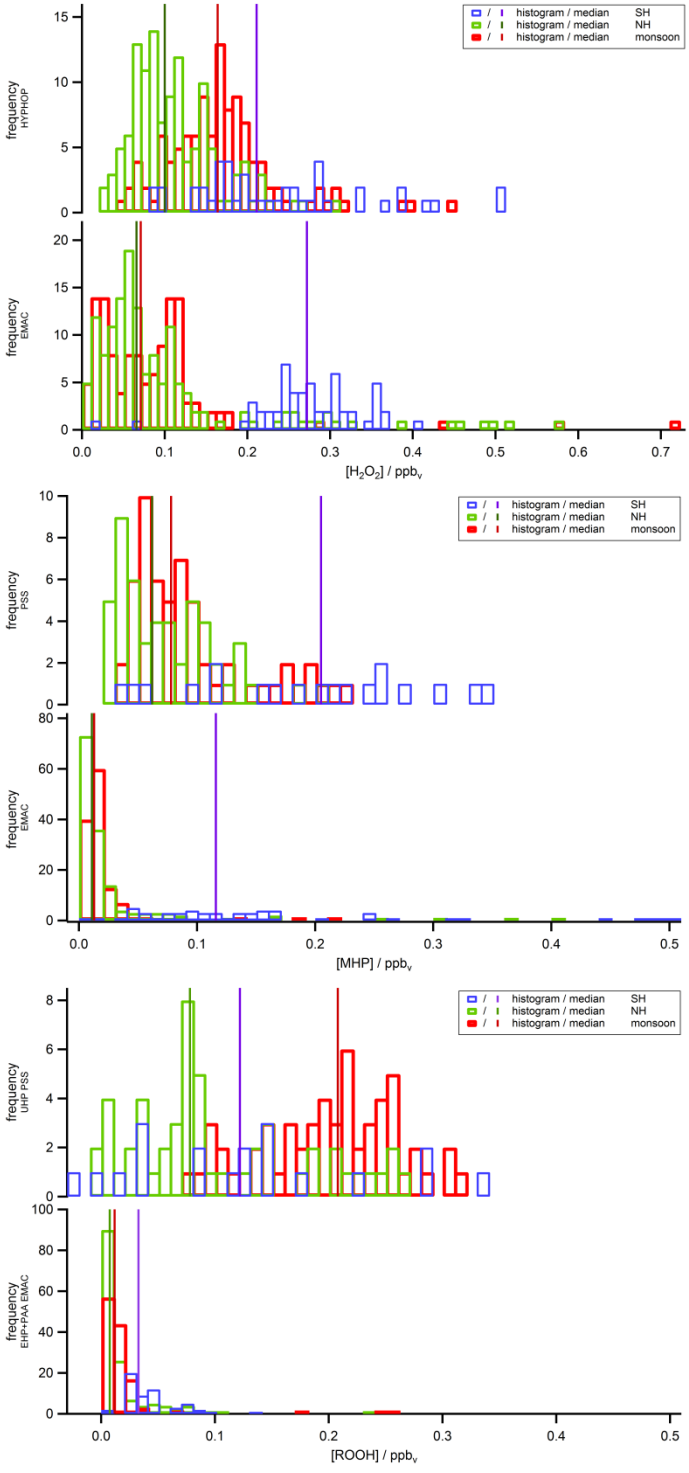

675

Figure 14: Histograms of observed and modelled H_2O_2 (top), MHP (middle) and UHP (bottom) mixing ratios during the OMO campaign for NH background (green), SH (blue) and AMA (red) air masses.

https://doi.org/10.5194/acp-2020-93
Preprint. Discussion started: 19 February 2020

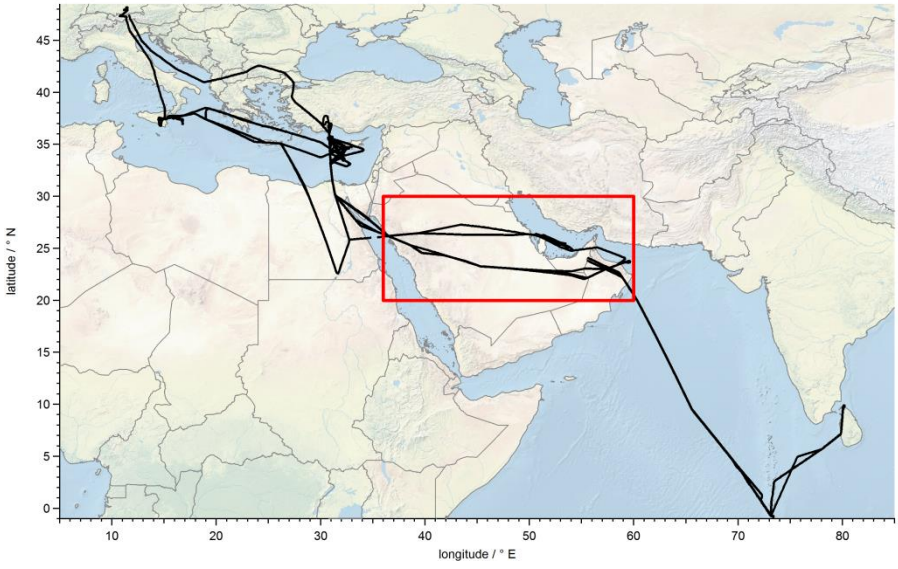

680

Figure 15: Location of measurements used for the longitudinal gradient study.

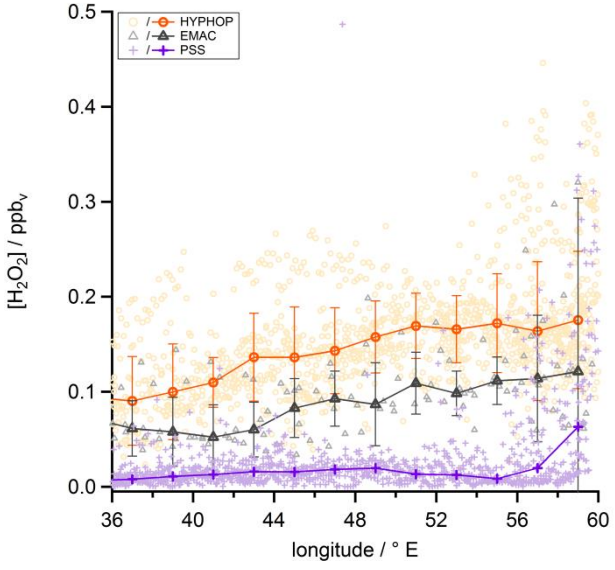

Figure 16: Longitudinal trends of H_2O_2 mixing ratios for observations (orange circles), EMAC (black triangles) and PSS (blue crosses). The data are shown in the light colors while the darker ones represent the medians.

https://doi.org/10.5194/acp-2020-93
Preprint. Discussion started: 19 February 2020

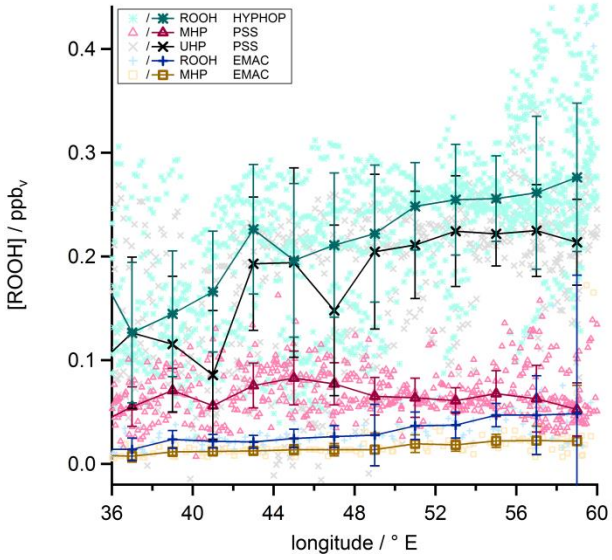

685

Figure 17: Longitudinal trends of ROOH mixing ratios for observations (green asterisks), EMAC (blue plus signs) and PSS mixing ratios for MHP (purple triangles) and UHP (black crosses) as well as EMAC MHP (yellow squares). The data are shown in the light colors while the darker ones represent the medians.

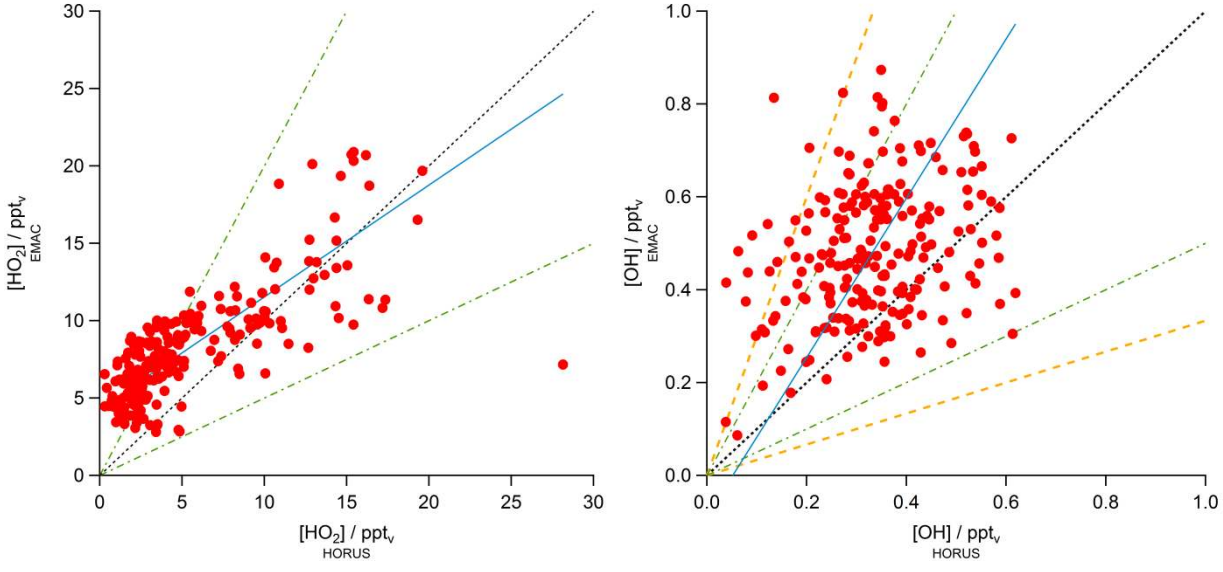

690

Figure 18: Scatter plot of *in situ* and modelled HO_2 data (left) and the OH data (right) (both red) with the 1:1 (black), 1:2 and 2:1 (both green) lines. The blue line shows the calculated least orthogonal distance fit.

https://doi.org/10.5194/acp-2020-93
Preprint. Discussion started: 19 February 2020

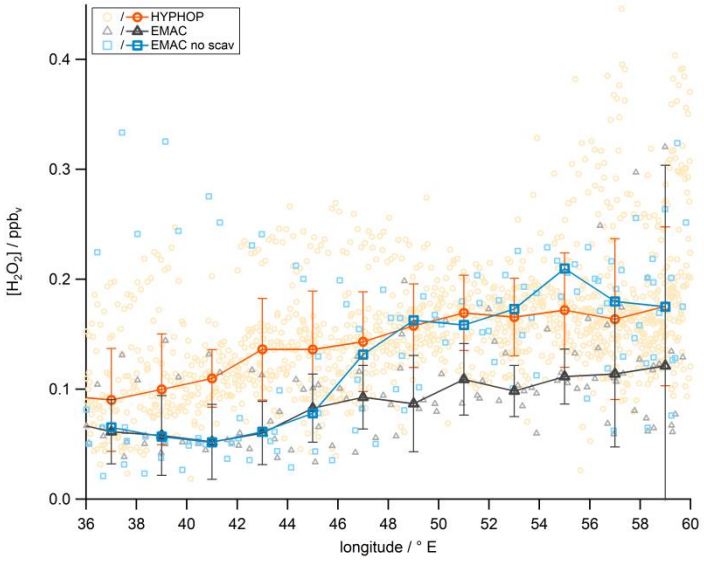

Figure 19: Longitudinal trends of H_2O_2 mixing ratios for observations (orange circles), EMAC (black triangles) and the sensitivity study without scavenging in EMAC (blue circles). The data are shown in the light colors while the darker ones represent the medians.

Table 1: Comparison of median H_2O_2, MHP and UHP mixing ratios in the upper troposphere from EMAC, measurements and calculations.

median	$[H_2O_2]/ppt_v$		$[MHP]/ppt_v$		$[UHP]/ppt_v$	
	EMAC	HYPHOP	EMAC	calc.	EMAC	calc.
NH background	66	115	11	64	8	89
monsoon	71	167	13	70	12	210
SH background	272	211	116	152	33	129